

RESEARCH ARTICLE | JANUARY 04 2011

# Macroporous photonic crystal-based vapor detectors created by doctor blade coating

Hongta Yang; Peng Jiang



*Appl. Phys. Lett.* 98, 011104 (2011)

<https://doi.org/10.1063/1.3535977>



CrossMark

## Articles You May Be Interested In

Superhydrophobic anti-ultraviolet films by doctor blade coating

*Appl. Phys. Lett.* (November 2014)

Macroporous photonic crystal-based anti-ultraviolet and anti-near-infrared materials by doctor blade coating

*Appl. Phys. Lett.* (February 2016)

Fabrication and photovoltaic property of ordered macroporous silicon

*Appl. Phys. Lett.* (October 2009)



A total solution for low-temperature characterization

[Learn more >](#)



# Macroporous photonic crystal-based vapor detectors created by doctor blade coating

Hongta Yang and Peng Jiang<sup>a)</sup>

Department of Chemical Engineering, University of Florida, Gainesville, Florida 32611, USA

(Received 29 November 2010; accepted 16 December 2010; published online 4 January 2011)

We report the achievement of rapid and reversible vapor detection by using 3D macroporous photonic crystals created by a continuous and scalable bottom-up technology. Capillary condensation of a condensable vapor in the interconnected macropores with  $\sim 74\%$  porosity leads to the increase of the effective refractive index of the diffractive medium, resulting in the redshift of the optical stop bands. The wavelength shift is linearly proportional to the vapor partial pressure for a spectrum of vapors. Optical simulation and theoretical prediction based on Kelvin equation suggest that a liquid film is formed on the walls of the macropores during vapor condensation. © 2011 American Institute of Physics. [doi:10.1063/1.3535977]

Mesoporous membranes, such as two-dimensional (2D) porous silicon and one-dimensional (1D) titania photonic crystals, have been widely used in sensitive vapor detection.<sup>1–14</sup> By monitoring the change of the optical properties (e.g., wavelength shift of the photonic band gaps or the Fabry–Perot fringes) of the diffractive media during vapor condensation, the concentration of the vapors can be deduced. Blue-colored *Morpho* butterfly wing scales, which are intrinsic three-dimensional (3D) photonic crystals exhibiting unique optical diffraction and interference, have also been demonstrated for highly selective vapor detection.<sup>15</sup> However, the limited size and material selection of these natural photonic crystals impede the development of reproducible and reusable vapor detectors. Here we show that 3D macroporous polymer photonic crystals created by an inexpensive and scalable bottom-up technology enable the rapid and reversible detection of a wide range of vapors ranging from water to toluene. The capillary condensation of vapors in the submicrometer-scale macropores, a topic that has received little examination,<sup>16–19</sup> has also been investigated by both experiments and theoretical calculations.

Macroporous polymer photonic crystals with 3D crystalline arrays of voids are fabricated by the scalable doctor blade coating technology.<sup>20</sup> Figures 1(a) and 1(b) show typical top-view scanning electron microscope (SEM) images of a DB-coated silica colloidal crystal-ethoxylated trimethylpropane triacrylate (ETPTA) polymer nanocomposite. The long-range hexagonal ordering of the colloidal crystal is clearly evident. The embedded silica microspheres can then be completely removed by etching in a 2 vol % hydrofluoric acid aqueous solution. After drying, the resulting self-standing macroporous polymer films exhibit uniform and shining colors caused by Bragg diffraction of visible light from 3D highly ordered air cavities [Figs. 1(c) and 1(d)]. Importantly, the large air cavities are interconnected through smaller windows [inset of Fig. 1(c)] which are originated from the touching sites of the close-packed silica microspheres in the shear-aligned nanocomposite.<sup>21</sup>

The templated macroporous polymer film is placed in a home-made environmental chamber. The chamber is evacu-

ated and then back-filled with a vapor with a specific pressure. Dry nitrogen is used to control the total pressure of the chamber to be 1 atm. An Ocean Optics (Dunedin, Florida) visible-near-IR spectrometer with a reflection probe is used for normal-incidence specular reflectance measurements. Absolute reflectivity is obtained as ratio of the sample spectrum and the reference spectrum, which is the optical density obtained from an aluminum-sputtered (1000 nm thickness) silicon wafer. Final value of the absolute reflectivity is the average of several measurements obtained from different spots on the sample surface.

Figure 2(a) shows the normal-incidence specular reflectance spectra obtained from a macroporous ETPTA film with 320 nm air cavities exposed to ethanol vapors with different partial pressures (from 0  $P_0$  to 1.0  $P_0$ ) at  $55 \pm 1$  °C.  $P_0$  is the saturation vapor pressure of ethanol at this temperature (280 mm Hg).<sup>22</sup> All spectra display distinct Bragg diffraction peaks with well-defined Fabry–Perot fringes, indicating high crystalline quality of the self-assembled macroporous photonic crystal. When the partial pressure of ethanol vapor is increased, ethanol condensates in the air cavities of the macroporous film, leading to a higher effective refractive index of the diffractive medium and a smaller dielectric con-

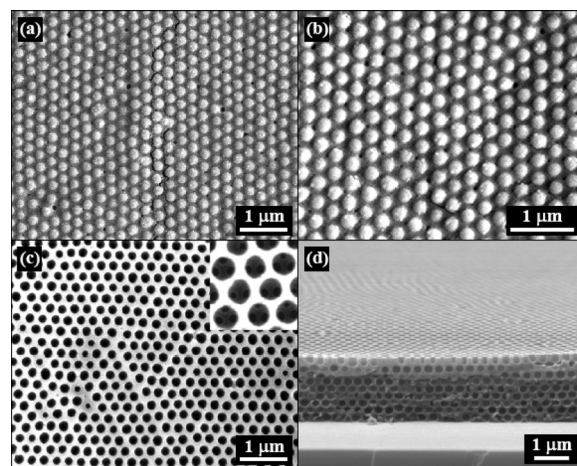


FIG. 1. (a) Top-view SEM image of a DB-coated silica colloidal crystal-polymer nanocomposite consisting of 320 nm silica spheres. (b) Magnified image of (a). (c) Top-view SEM image of a templated macroporous polymer film. Inset showing a magnified portion of the film. (d) Cross-sectional SEM image of the same sample as in (c).

<sup>a)</sup> Author to whom correspondence should be addressed. Electronic mail: pjiang@che.ufl.edu.

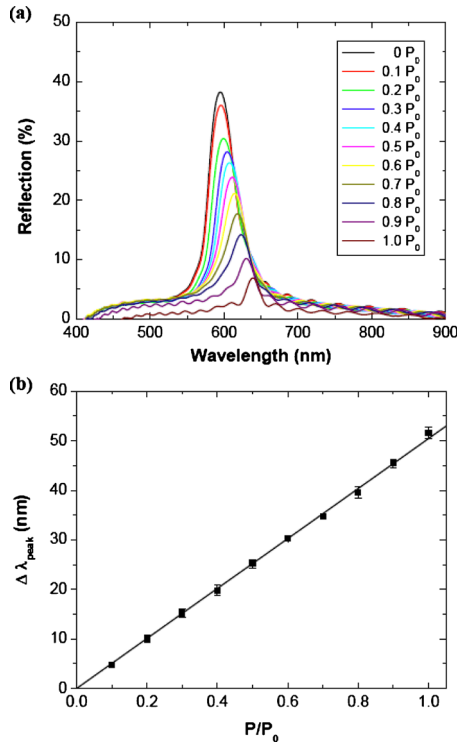


FIG. 2. (Color online) (a) Normal-incidence specular reflection spectra obtained from a macroporous polymer film consisting of 320 nm air cavities exposed to ethanol vapors with different partial pressures. (b) Dependence of the shift of the Bragg diffraction peak vs ethanol partial pressure.

trast between the polymer and the enclosed materials. This explains the observed redshift of the Bragg diffraction peaks and the reduction of the amplitude of the optical stop bands. Figure 2(b) indicates that the shift of the diffraction peaks (compared to the sample exposed to pure nitrogen gas) is nearly linear with respect to the ethanol partial pressure. By monitoring the time dependence of specular reflectance spectra at difference vapor partial pressures and temperatures, the speed of response (i.e., time to reach equilibrium) of photonic crystal vapor detectors is determined to be less than 1 min. The optical properties of the macroporous polymer films are fully recovered when the condensed ethanol is evaporated. The photonic crystal films can thus be reused many times for reproducible vapor detection.

To gain a better understanding of vapor condensation in templated macroporous films, we calculate the amount of condensed ethanol at different vapor partial pressures by using the Bragg diffraction equation  $\lambda_{\max} = 2 \times n_{\text{eff}} \times d \times \sin \theta$ , where  $n_{\text{eff}}$  is the effective refractive index of the diffractive medium,  $d$  is the interplane distance, and  $\theta$  is  $\pi/2$  for normal incidence. By assuming the templated air cavities are close-packed and the volume fraction (VF) of air in a dry macroporous polymer film is 0.74, the effective refractive index of the medium can be calculated as  $n_{\text{eff}} = n_{\text{ETPTA}} \times 0.26 + n_{\text{air}} \times \text{VF}_{\text{air}} + n_{\text{EtOH}} \times (0.74 - \text{VF}_{\text{air}})$ , where  $n_{\text{ETPTA}}$ ,  $n_{\text{air}}$ , and  $n_{\text{EtOH}}$  are 1.46, 1.0, and 1.36, respectively. The calculated volume fractions of the remaining air ( $\text{VF}_{\text{air}}$ ) in the macroporous film at different ethanol partial pressures are shown in Fig. 3(a).

If we assume the condensed ethanol forms a uniform thin liquid layer on the walls of the polymer voids, the thickness of this ethanol layer can be calculated by using the volume fraction of the condensed ethanol ( $0.74 - \text{VF}_{\text{air}}$ ). The

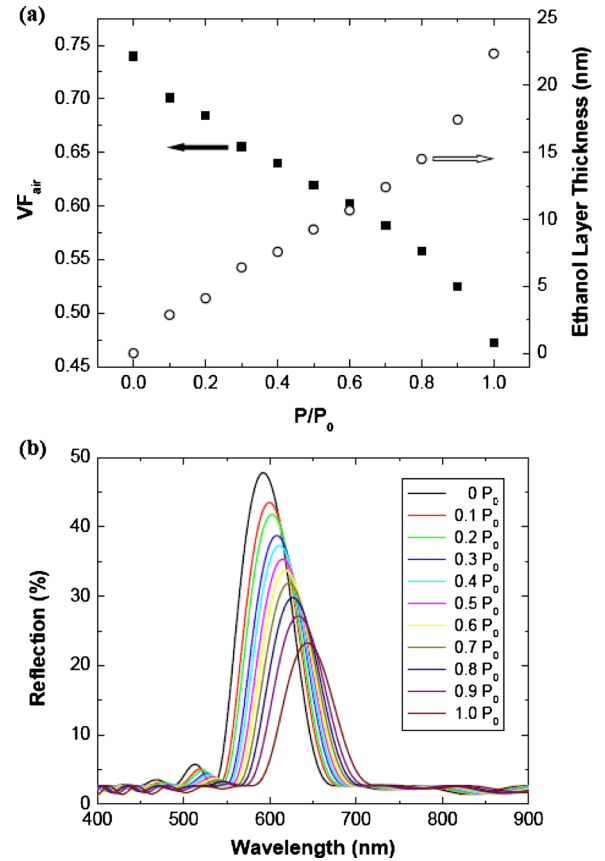


FIG. 3. (Color online) (a) Calculated volume fractions of air and the corresponding adsorbed ethanol layer thickness at different ethanol partial pressures. (b) Simulated specular reflection spectra obtained from a macroporous polymer film consisting of 320 nm cavities exposed to ethanol vapors with different partial pressures.

results in Fig. 3(a) show that a 22.4 nm liquid layer can be formed on the walls of 320 nm voids when the macroporous film is exposed to a saturated ethanol vapor. The calculated ethanol layer thickness is then incorporated in the scalar wave approximation model<sup>23</sup> developed for periodic dielectric structures to quantitatively simulate the specular reflectance spectra at different vapor partial pressures. Although the simulated spectra [Fig. 3(b)] exhibit higher reflectance than the experimental results [Fig. 2(a)], the shape, position, redshift, and amplitude reduction of the diffractive peaks associated with the condensation of ethanol in the voids of the macroporous photonic crystal agree well with the experiments.

We attribute the condensation of ethanol vapor in the macroporous photonic crystals to capillary condensation. The Kelvin equation,

$$\ln \frac{P}{P_0} = - \frac{2\gamma V_l}{rRT},$$

where  $P$  and  $P_0$  are actual and saturation vapor pressure,  $\gamma$  is the liquid/vapor surface tension,  $V_l$  is the liquid molar volume,  $r$  is the radius of curvature, can be used to describe the phenomenon of capillary condensation due to the presence of a curved meniscus.<sup>18,19</sup> In macroporous films, the radius of curvature of the condensed liquid film equals to the radius of the air cavity minus the liquid film thickness. Thus a higher vapor partial pressure leads to a smaller  $r$  (i.e., a thicker liquid layer). In addition, as  $\gamma$ ,  $V_l$ ,  $R$ , and  $T$  are all constants

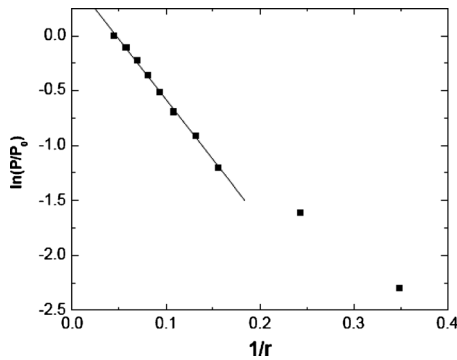


FIG. 4. Dependence of  $\ln(P/P_0)$  vs the reciprocal of the radius of curvature of the condensed liquid films.

at a fixed temperature,  $\ln(P/P_0)$  is inversely proportional to  $r$ . Figure 4 shows that this prediction agrees well with experimental results when the liquid layer is relatively thick. A thinner liquid layer formed at a low vapor partial pressure might not be continuous and this could explain the large deviation of the two data points in Fig. 4.

The macroporous photonic crystal-based vapor detection can be easily extended to a large variety of vapors, such as toluene and water. Figure 5 shows that the response of water detection is quite familiar with that of ethanol detection. It is noteworthy to mention that a bulk liquid water droplet can-

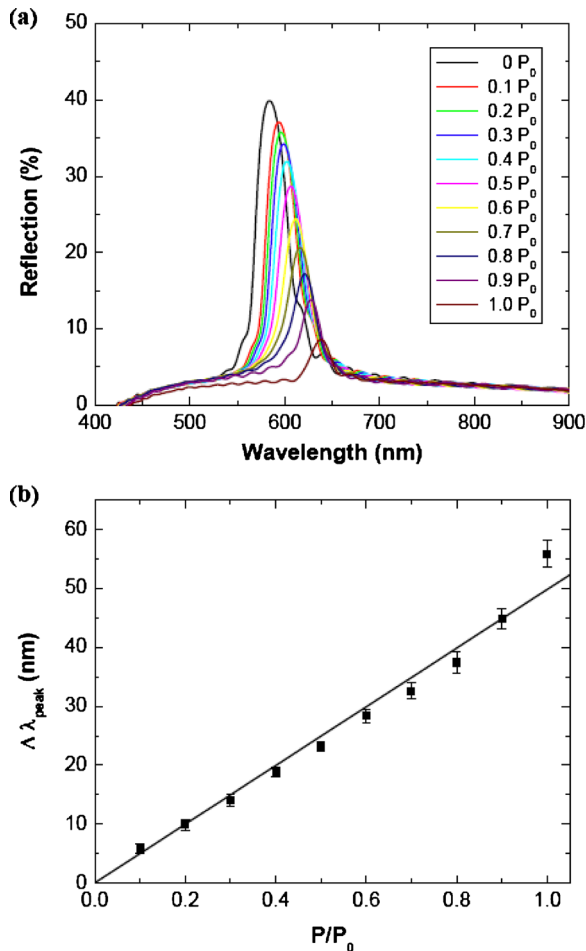


FIG. 5. (Color online) (a) Normal-incidence specular reflection spectra obtained from a macroporous polymer film consisting of 320 nm air cavities exposed to water vapors with different partial pressures. (b) Dependence of the shift of the Bragg diffraction peak vs water partial pressure.

not penetrate into the voids of a templated macroporous ETPTA film due to a large water contact angle of  $78 \pm 3^\circ$ .

Above we have shown that macroporous photonic crystal-enabled vapor detectors can sense vapors at both high and low concentrations. The flexible macroporous polymer membranes, which can be scalably and economically produced over large areas by the doctor blade coating technology, could be applicable as low-cost, portable colorimetric vapor sensors (e.g., humidity sensors) at relatively high concentrations. To increase the sensitivity of the templated macroporous vapor detectors at low concentration, the full-spectrum analysis technique, which considers both the shift of the optical stop bands and the change of the spectral amplitude, can be applied. To enhance the selectivity for mixtures of vapors, the polymer surface can be selectively modified or hierarchical structures (e.g., multiple layers with each layer responding to a specific vapor) can be explored.<sup>15</sup>

In summary, we have demonstrated that macroporous photonic crystals created by a continuous and scalable doctor blade coating process can be used directly for vapor detection. The capillary-condensed vapor forms a liquid layer covering the surface of the submicrometer-scale macropores.

This work was supported by DTRA and NSF under Grant Nos. CBET-0744879 and CMMI-1000686.

- <sup>1</sup>L. De Stefano, L. Moretti, A. Lamberti, O. Longo, M. Rocchia, A. M. Rossi, P. Arcari, and I. Rendina, *IEEE Trans. Nanotechnol.* **3**, 49 (2004).
- <sup>2</sup>T. Endo, Y. Yanagida, and T. Hatsuzawa, *Sens. Actuators B* **125**, 589 (2007).
- <sup>3</sup>X. Y. Fang, V. K. S. Hsiao, V. P. Chodavarapu, A. H. Titus, and A. N. Cartwright, *IEEE Sens. J.* **6**, 661 (2006).
- <sup>4</sup>N. Hidalgo, M. E. Calvo, S. Colodrero, and H. Miguez, *IEEE Sens. J.* **10**, 1206 (2010).
- <sup>5</sup>T. Hutter and S. Ruschin, *IEEE Sens. J.* **10**, 97 (2010).
- <sup>6</sup>T. Karacali, M. Alanyalioglu, and H. Efeoglu, *IEEE Sens. J.* **9**, 1667 (2009).
- <sup>7</sup>B. H. King, A. Gramada, J. R. Link, and M. J. Sailor, *Adv. Mater. (Weinheim, Ger.)* **19**, 4044 (2007).
- <sup>8</sup>B. H. King, A. M. Ruminski, J. L. Snyder, and M. J. Sailor, *Adv. Mater. (Weinheim, Ger.)* **19**, 4530 (2007).
- <sup>9</sup>J. Kobler, B. V. Lotsch, G. A. Ozin, and T. Bein, *ACS Nano* **3**, 1669 (2009).
- <sup>10</sup>I. A. Levitsky, W. B. Euler, N. Tokranova, and A. Rose, *Appl. Phys. Lett.* **90**, 041904 (2007).
- <sup>11</sup>V. S. Y. Lin, K. Moteshareh, K. P. S. Dancil, M. J. Sailor, and M. R. Ghadiri, *Science* **278**, 840 (1997).
- <sup>12</sup>A. M. Ruminski, M. M. Moore, and M. J. Sailor, *Adv. Funct. Mater.* **18**, 3418 (2008).
- <sup>13</sup>H. Saha and C. Pramanik, *Mater. Manuf. Processes* **21**, 239 (2006).
- <sup>14</sup>M. S. Salem, M. J. Sailor, F. A. Harraz, T. Sakka, and Y. H. Ogata, *J. Appl. Phys.* **100**, 083520 (2006).
- <sup>15</sup>R. A. Potyrailo, H. Ghiradella, A. Vertiatikh, K. Dovidenko, J. R. Cournoyer, and E. Olson, *Nat. Photonics* **1**, 123 (2007).
- <sup>16</sup>S. J. Gregg and K. S. W. Sing, *Adsorption, Surface Area and Porosity*, 2nd ed. (Academic Press Inc., London, 1982).
- <sup>17</sup>B. Coasne, A. Grosman, C. Ortega, and M. Simon, *Phys. Rev. Lett.* **88**, 256102 (2002).
- <sup>18</sup>L. R. Fisher, R. A. Gamble, and J. Middlehurst, *Nature (London)* **290**, 575 (1981).
- <sup>19</sup>Z. Gemici, P. I. Schwachulla, E. H. Williamson, M. F. Rubner, and R. E. Cohen, *Nano Lett.* **9**, 1064 (2009).
- <sup>20</sup>H. T. Yang and P. Jiang, *Langmuir* **26**, 13173 (2010).
- <sup>21</sup>A. Blanco, E. Chomski, S. Grabtchak, M. Ibisate, S. John, S. W. Leonard, C. Lopez, F. Meseguer, H. Miguez, J. P. Mondia, G. A. Ozin, O. Toader, and H. M. van Driel, *Nature (London)* **405**, 437 (2000).
- <sup>22</sup>D. R. Lide and H. P. R. Frederikse, *CRC Handbook of Chemistry and Physics*, 76th ed. (CRC, Boca Raton, FL, 1995).
- <sup>23</sup>Z. Zhang and S. Satpathy, *Phys. Rev. Lett.* **65**, 2650 (1990).